OPTOELECTRONICS AND ADVANCED MATERIALS – RAPID COMMUNICATIONS Vol. 12, No. 11-12, Nov.-Dec. 2018, p. 687 - 693

Fabrication of perovskite solar cells in ambient air by employing poly (triarylamine) as the hole transport layer

GUILIN LIU[a,b,c], XI XI[a], WEIFU DONG[b,c]
[a]*School of Science, Jiangnan University, WuXi, China, 214122*
[b]*School of Chemical and Materials Engineering, Jiangnan University, Wuxi, China, 214122*
[c]*National International Joint Research Center for Photoresponse Functional Molecular Materials, Jiangnan University, Wuxi, China, 214122*

Poly-(triarylamine) (PTAA) was employed as the hole transport layers (HTLs) to fabricate perovskite solar cells (PSCs) in ambient air wherein the temperature and relative humidity were controlled at 30 ℃ and 30%, respectively. In comparison to PSCs based on spiro-OMeTAD HTLs, the statistical power conversion efficiency (PCE) of ambient-air-fabricated solar cells was close to solar cells which were fabricated in nitrogen. It indicated the PTAA layers were less sensitive in air than that of spiro-OMeTAD during the fabrication process. The PCE was around 12% in average for PSCs with PTAA HTLs. Additionally, it was found that oxygen aging can further improve the PCE to 14% in average. However, though the stability of HTLs were improved by employing PTAA, the perovskite crystals limits the long-term stability of perovskite solar cells. According to our experiments, after 2-weeks degradation in air, the PCE of all PSCs were dropped due to the decomposition of perovskite crystals. As a result, additional encapsulation treatments are worthy investigated for the long-term stability of perovskite solar cells.

(Received February 27, 2018; accepted November 29, 2018)

Keyword: Solar energy materials, Hole transport layer, Ambient air

1. Introduction

Organic/inorganic hybrid lead halide perovskite (PVSK) solar cells (PSCs) have attracted much attention because of high power conversion efficiency (PCE) [1-6] and are expected to further increase. Though advantages [7-13], such as low-cost and high PCE, have been widely acknowledged, plenty details of PSCs still need to be fully investigated. Among those issues, the Hole Transport Layer (HTL) [14-16] is an important factor which significantly limits the PCE and the cost. For an example, 2, 2′, 7, 7′-tetrakis [*N*, *N*-di (4-methoxyphenyl) amino]-9, 9′- spirobifluorene (spiro-OMeTAD) [17-19] has been widely used as Hole Transport Materials (HTMs) due to its high conductivity and suitable bandgap. However, the spiro-OMeTAD solution contains both spiro-OMeTAD and Lithium bis (trifluoromethyl sulfonyl)-imide (Li-TFSI) in high concentration, which dramatically increased the experimental expense. Moreover, devices sequential need to be aged in pure oxygen cabin for over 12 hours [20] because the carrier mobility of spiro$^+$ was higher than intrinsic spiro-OMeTAD [19]. The aging treatment also goes far when it was contrasted with the expectation of industralization. Meanwhile, most literatures have declared that PSCs [20-22] should be fabricated and characterized in an extremely clean environment, such as in nitrogen filled glovebox, to prevent oxygen and moisture permeation. To simplify those complicated processes, we have investigated poly (triarylamine) (PTAA) [23] as HTM because its efficient hole transport ability and high stability in air, aiming to simplify the fabrication processes of PSCs.

In this letter, a fast solution fabrication method was introduced which most fabrication processes can be carried out in air condition except the sliver evaporation. During the fabrication process, the key point here is to keep the Relative Humidity (RH) and Temperature at around 30% and 30 ℃, respectively. All spin-coating and annealing processes were carried out in ambient air for solar cells based on PTAA HTLs. In Contrast, PSCs with spiro-OMeTAD HTLs were all fabricated in nitrogen filled glove box. A rapid fabrication method was exploited through comparing conditions of ambient air and nitrogen atmosphere. Obviously, ambient air was easier for the further industrialization. However, it is widely known [20-22] that oxygen and moisture in air can dramatically decrease the PCE of PSCs. Differently, we have found that ambient-air-fabricated PSCs show an acceptable performance comparing with PSCs fabricated in nitrogen condition. Even more, it was found that short-time oxygen aging has a potential improvement for PSCs with PTAA HTLs. However, the long-term stability was dropped when samples were placed in ambient air due to the decomposition of perovskite crystals. Hence, additional encapsulation technique was also worthy investigated after the device fabrication.

2. Experimental

2.1. Device fabrication

The ITO substrates (7Ω/☐, Nanbo INC.) were sequentially dual cleaned with isopropanol (AR, Sinopharm), acetone (AR, Sinopharm), ethanol (AR, Sinopharm), distilled water (Milli-Q INC.) in ultrasonic bath. After UV treatment, Tin (IV) oxide (SnO_2, 15% in H_2O colloidal dispersion, Alfa Aesar) were then spin-coated on substrates as Electron Transport Layer (ETL) and annealed at 150 ℃ for 30 min in ambient air. Methylamine iodide (MAI, ≥ 99%, Sigma Aldrich) and Lead (II) iodide (PbI_2, 99.999%, Sigma Aldrich) were solved in N, N-Dimethylformamide (DMF, 99.8% Sigma Aldrich) as precursor solution before spin-coating process. After the temperature of substrates were dropped to room temperature, Methylamine-Lead(II) -iodide ($MAPbI_3$) precursor solution was then spin-coated on ETL as active layer at 3000 rpm for 20 s, 500 μL of diethyl ether was dripped (before end of the 14 s) on films during the spin-coating. Substrates were immediately moved to hot plate for 10 min annealing at 75 ℃ to form the perovskite structure. Both PTAA ($M_n \geq 7000$, Sigma Aldrich) and spiro-OMeTAD (99%, Sigma Aldrich) were employed as HTMs, respectively. The first sets of PTAA solution (nominated as PTAA1) was prepared by dissolving 10 mg of PTAA in toluene (10 mg/mL, 99.8%, Sigma Aldrich) with 7.5 μL Li-TFSI (99.95%, Sigma Aldrich) in acetonitrile (170 mg/mL, 99.8%, Sigma Aldrich) and 4 μL 4-tert-butylpyridine (TBP, 96%, Sigma Aldrich). The second sets of PTAA (nominated as PTAA2) was prepared by dissolving 10 mg of PTAA in toluene (10 mg/mL) with 13 μL Li-TFSI in acetonitrile (28.3 mg/mL) and 4 μL TBP, respectively. Spiro-OMeTAD solution was prepared by dissolving 72.3 mg of spiro-OMeTAD, 28.9 μL of TBP, and 17.5 μL of a stock solution of 520 mg/mL Li-TFSI in acetonitrile in 1 mL of Chlorobenzene (99.8%, Sigma Aldrich). It is important to note that, except sliver evaporation, all layers were fabricated in ambient air for devices which were employed PTAA as HTLs. The Temperature and RH was kept under 30 ℃ and 30% during the experiments. In Contrast, Devices with spiro-OMeTAD HTLs were all fabricated in nitrogen filled glove box including the fabrication of ETLs. Finally, the 100 nm counter electrode was deposited by thermal evaporation of sliver (99.99% Kurt J. Lesker) under a pressure of 3.5×10^{-5} Pa. The effective area was 0.102 cm^2. The as-fabricated devices consist of five functional cells as shown in Fig. 1.

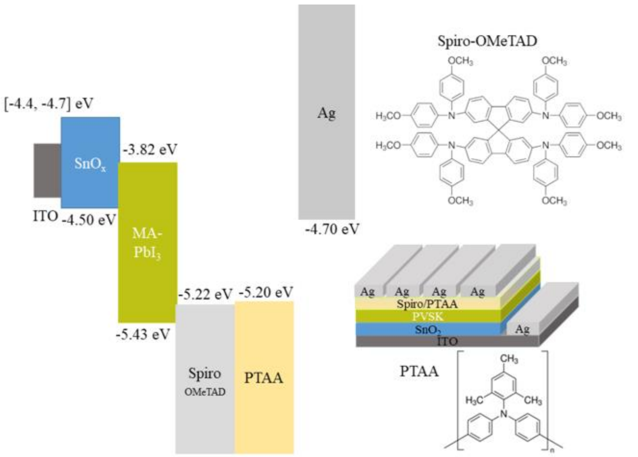

Fig. 1. Schematic figure of PSCs

2.2. Device characterization

The X-ray diffraction (XRD) spectrum of ITO/PVSK film was measured using a PANalytical X-ray Diffractometer with Cu k_α radiation at a scanning rate(2θ) of 3 $°min^{-1}$. The accelerating voltage and current were 40 kV and 40 mA, respectively. UV/visible (UV/vis) absorption spectrum was recorded in Hitach (Model U3900) spectrometer at a rate of 0.5 nm/s. The Photocurrent-Voltage (J-V) measurement for the perovskite solar cells were performed under AM 1.5 G irradiation (100 mW/cm^2) using a Xenon lamp simulator (Enlitech, model SS-F7-3A) with a shadow mask area of 0.102 cm^2. The External Quantum Efficiency (EQE) was measured by tunable monochromic light source (Enlitech, model QE-R). Cross-sectional image was measured by FE-SEM (Hitachi, S-4800FESEM) operated at 5 kV.

3. Results and discussion

Crystal quality of PVSK films is a vital role on devices. Especially all coating processes of PTAA sets in our experiments were fabricated in air. For one-step method, diethyl ether was used to speed up PVSK nucleation via an instantaneous supersaturation during the spin-coating of precursor solution [24]. Usually PVSK films were coated and annealed in insert nitrogen glove box [20-22], because of the instability of PVSK film with oxygen and moisture. To simplify the fabrication process, all spin-coating and annealing methods were carried out in ambient air with controlled temperature and humidity. The XRD and UV/vis absorption spectrum were instantly characterized after the annealing of PVSK films. Fig. 2 represented XRD and UV/vis spectrum of $MAPbI_3$ PVSK films, respectively. As shown in Fig. 2 (a), diffraction peaks were assigned to lattice plane (110), (220), (310), respectively. It confirmed that a tetragonal structure of $MAPbI_3$ was formed. This result was in accordance with with Wu [25]. Fig. 2 (b) displayed UV/vis absorption spectrum of $MAPbI_3$ thin film, PVSK crystalline had a wide absorption band in visible region with a cutoff edge at around 780 nm. The onset peak was around 1.6 eV corresponded to the bandgap of $MAPbI_3$. The bandgap result indicated that spin-coating and anneal in ambient air have slight impact on the crystal quality and the fermi energy. Compared to other literatures [21, 25], either crystallization quality or absorption band changed once the perovskite crystals were fabricated in air.

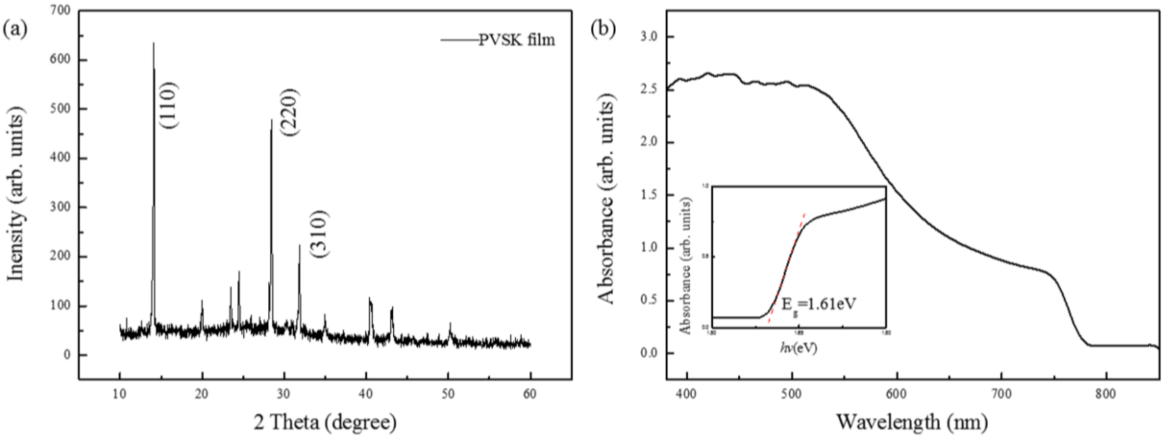

Fig. 2. (a) X-ray diffraction pattern of PVSK film which exhibited a tetragonal structure; (b) UV-vis absorption spectrum of $MAPbI_3$ film on ITO substrate

Cross-section morphology of films was also an important issue for the PVSK films. After the annealing treatment, PTAA and spiro-OMeTAD were respectively spin-coated as HTL in different atmosphere (ambient air and pure nitrogen). Cross-section images were characterized using a field emission-scanning electron microscope after the sliver evaporation. Cross-section images were shown in Fig. 3. Although group of films were spin coated in ambient air, all layers were integrated closely with each other, providing smooth interfaces for charge transportation. Also, pinholes and ionic diffusions were invisible in SEM images which have provided direct evidence that oxygen and humidity infiltration can be eliminated by controlling temperature and humidity.

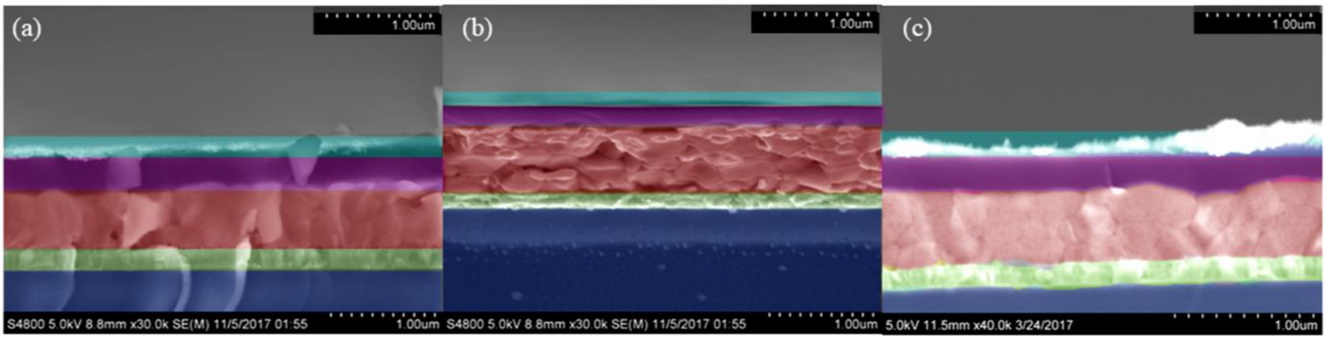

Fig. 3. SEM micrographs of ITO/SnO_2/$MAPbI_3$/HTL/Ag cross-sections. (a) was the cross section image of the PSCs based on the 1st sets of PTAA that we have mentioned in experimental section, while in (b) was the cross-section of the 2ed sets of PSCs, (c) displays the solar cells based on HTL of spiro-OMeTAD. Samples from (a) and (b) were fabricated in ambient air and (c) was fabricated in nitrogen glove box

The photovoltaic properties of the $MAPbI_3$ PVSK devices were sequentially characterized under solar simulator after the sliver evaporation. Devices with PTAA HTLs were immediately measured after metal electrode deposition. On the other hand, after 12-hour sealing in pure oxygen, PSCs with spiro-OMeTAD HTLs were then characterized under AM 1.5G irradiation. All parameters were summarized over 20 pieces of solar cells for each set in order to guarantee the accuracy. All results were shown in Fig. 4 and Table 1. Tough the PCE can be further improved, the statistical results were in accordance with the original assumption that fabrication processes are possible to be simplified and carried out in ambient air. According to statistical photovoltaic results, PSCs with HTLs based on PTAA (sets of PTAA1) have a comparable PCE than that of spiro-OMeTAD based HTLs. The statistical PCE in average was around 12% if the additive of Li-TFSI was increased to 1.275 mg in the solution.

Contrasted with spiro-OMeTAD, samples with PTAA HTLs were all fabricated in ambient air except the sliver deposition. Conversely, although all layers were fabricated in pure nitrogen and high vacuum conditions, The PCE of PSCs with spiro-OMeTAD HTLs were slightly over 10%. Meanwhile, it was found that temperature, RH and oxygen strongly influenced the performance if Li-TFSI reduced from 1.275 mg to 0.368 mg. It represented that the concentration of Lithium salt is vital to the PTAA HTL film quality. On the other hand, the Open-Circuit Voltage (V_{oc}) of PSCs with spiro-OMeTAD HTLs was fluctuated, even though all processes were fabricated in nitrogen filled glove box. As seen from Fig. 4, Fill Factor (FF) and short circuit current (J_{sc}) also significantly influenced the PCE performance. According to Fig. 4, the concentration of Lithium salt was the main reason for the performance of PSCs because all other material concentrations between two sets of PTAA layers were exactly the same. Marumoto has reported [26] that Li-TFSI dopant has strongly effects on spiro-OMeTAD films. However, each spiro-OMeTAD film contains almost 10 mg Li-TFSI which is almost an order of magnitude higher than that of PTAA films. Moreover, PSCs with spiro-OMeTAD layers require over additional 12 hours in oxygen [20] for aging. In comparison to the PCE performance, though the FF was fluctuated for PSCs with PTAA HTLs, these efforts of ambient air methods were worth considering for the future industrial application.

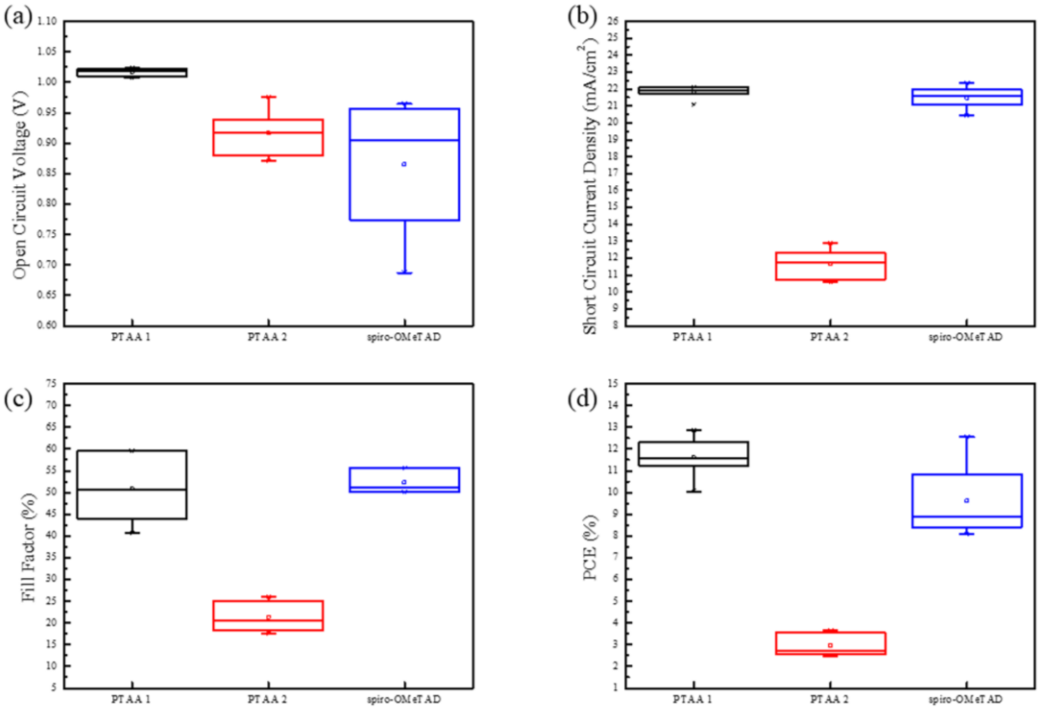

Fig. 4. Statistical J-V parameters of PSCs. (a), (b) and (c) were statistical open-circuit voltage, Fill Factor and short circuit current density, respectively. (d) represented the statistical results of PCE

Table 1. Solar cell performance parameters extracted from J-V characteristics in Fig. 4. In each set, 20 pieces of solar cells were characterized to guarantee the accuracy

Parameters	PCE (%)		V_{oc} (V)		FF (%)		J_{sc} (mA/cm2)	
Cell type	Average	Max	Average	Max	Average	Max	Average	Max
PTAA1	11.60	12.86	1.01	1.02	50.80	59.51	21.82	22.13
PTAA2	2.95	3.64	0.91	0.98	21.38	26.02	11.65	12.90
spiro	9.62	12.55	0.87	0.96	52.33	55.62	21.49	22.35

The best PCE in each set were plotted in Fig. 5. The PCE of solar cells was dramatically decreased when the concentration of Li-TFSI was dropped to a quarter in PTAA HTL. It indicated that Lithium salt played a dominant role in charge transportation. The decrease of FF was directly related [27]to the charge extraction, especially the hole extraction. Meanwhile, though spiro-OMeTAD solution contained high concentration of Li-TFSI, the PCE was close to PSCs based on PTAA HTLs (sets of PTAA1). The EQE also confirmed that the difficulty of hole extraction if the concentration of Li-TFSI was decreased in PTAA HTLs. The photocurrent decreased by 10 mA/cm^2 once the lithium additive was dropped from 1.275 to 0.368 mg per milliliter in PTAA solution. On the other hand, though all devices were aged 12 hours in oxygen and contained 9.1 mg Li-TFSI in solution for the experimental sets of spiro-OMeTAD HTLs, the integrated photocurrent was close to PSCs with PTAA HTLs. This result indicated that the PTAA was a feasible HTM rather than spiro-OMeTAD.

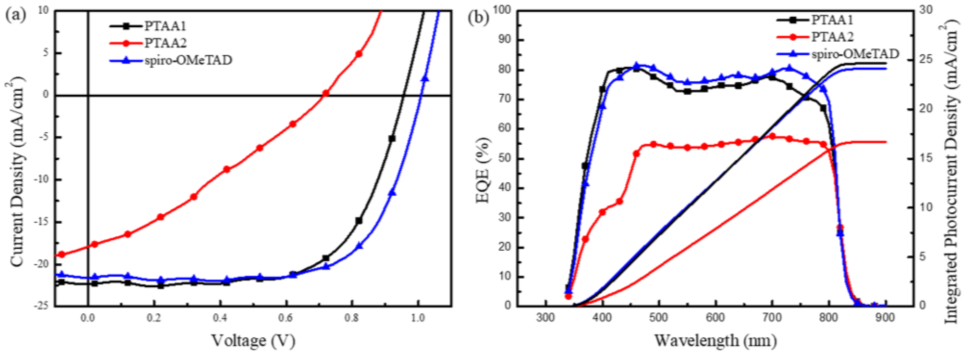

Fig. 5. (a) best J-V curves of ITO/SnO$_x$/MAPbI$_3$/HTL/Au structure of cells using PTAA and spiro-OMeTAD HTLs. (b) EQE and integrated photocurrent as a function of wavelength (nm) for the devices

After EQE characterization, then all devices with PTAA HTLs were then aged over 12 hours in oxygen condition at room temperature. It can be seen from Fig. 6, the average PCE was significantly increased to 14% in average indicating that PTAA HTL conductivity can be further improved after oxygen aging treatment. However, the V_{oc} was significantly decreased and fluctuated after oxygen treatment. Meanwhile, J_{sc} was slightly increased after the aging treatment. Hence, the PCE improvement was mainly from increased FF. Though the aging mechanism in PTAA HTL is unclear, Li-TFSI probably plays a dominant factor according to previous research [26]. Back to our research, we mainly provided a rapid fabrication method for PSCs based on PTAA HTLs.

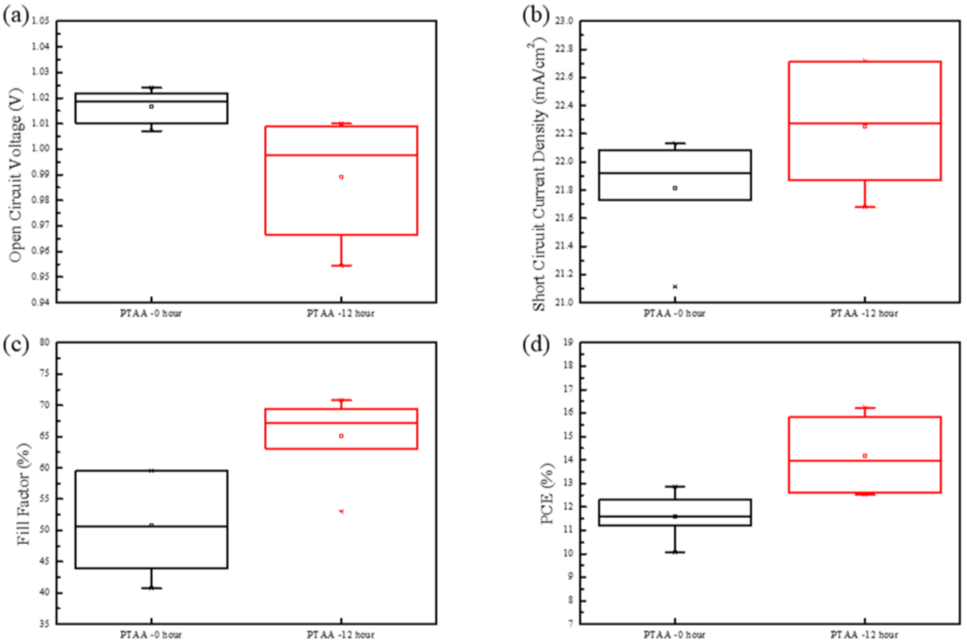

Fig. 6. Statistical photovoltaic parameters before and after oxygen aging treatment

Additionally, the long-term stability of PSCs was characterized after each 7 days. All samples were kept in air condition after fabrication without encapsulation. The results were shown in Fig. 7. It can be seen that all samples degraded in air. The PCE of PSCs with PTAA HTLs was gradually dropped over 50% compared to the pristine cells. Meanwhile, the PCE of PSCs with spiro-OMeTAD HTLs also decreased from 10% in average to 6%. This indicated that the degradation of perovskite crystals played a dominate role in long-term stability rather than the HTM aging. According to previous investigations [28], the MA^+ cations were sensitive to humidity. Once H_2O was adsorbed on to the perovskite crystals, the MA^+ cations would instantly be converted to CH_3NH_3OH. Meanwhile, excess H^+ then can easily destroy the sliver electrodes because iodide (I^-) can bond with sliver which finally formed silver iodide (AgI), leading to the PCE decrease. Hence, additional treatments such as encapsulation are worthy investigated to increase the long-term stability for perovskite solar cells.

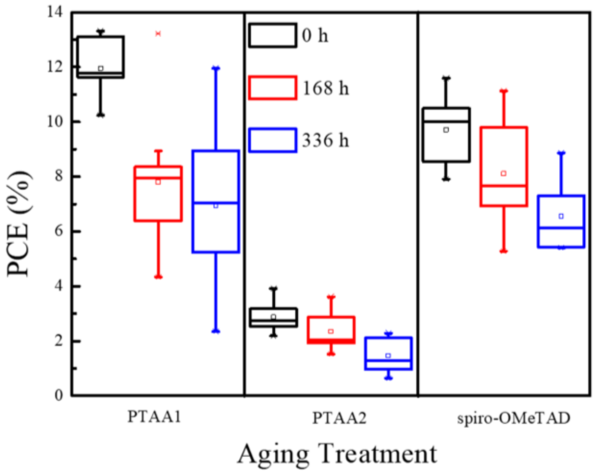

Fig. 7. The PCEs of PSCs of each sets. The performances were characterized after each 7 days. All devices were kept in air without encapsulation

4. Conclusion

This work presents a fast fabrication process on the photovoltaic of $MAPbI_3$ by applying PTAA as hole transport layer. All spin-coating and annealing methods were carried out in ambient condition. The PCE performance remained in stable if temperature and RH was controlled around 30 ℃ and 30%, respectively. The fabrication process then can be significantly simplified than that of in nitrogen sealed conditions. Based on this fabrication method, PSCs showed a comparable PCE around 12% in average. Moreover, the PCE was even achieved to 14% in average after the oxygen aging. Herein, this method can also introduce to other optoelectrical manufactures including light-emitting diodes and laser fabrication, which have recently involved the promising hybrid organic-metal halide perovskite material. However, the long-term stability of PSCs was decreased once samples were placed in air without encapsulation. It was found that the decomposition of MA^+ cations was the key point for the stability, due to the adsorption of water in air. As a result, additional treatments such as encapsulation were worthy investigated for the long-term stability of perovskite solar cells which can protect the stability of perovskite crystals.

Acknowledgement

The project is supported by the Natural Science Foundation of Jiangsu Province, China (Grant No. BK20180601), (Grant No. BK20180596), the Fundamental Research Funds for the Central Universities (JUSRP11834), (JUSRP11834B), and Jiangsu Postdoctoral Science Foundation (2018K112C) (2018K113C). We sincerely thank Enlitechnology for offering the steady-state solar simulator.

References

[1] C. Bi, B. Chen, H. Wei, J. Huang, et al., Advanced Materials **29**, 1605900 (2017).
[2] J. H. Heo, M. Graztel, S. Seok, et al., Nature Photonics **7**(7), 486 (2013).
[3] H. Zhou, Q. Chen, Y. Yang, et al., Interface Engineering of Highly Efficient Perovskite Solar Cells **345**(542), 1254050 (2014).
[4] W. Sun, C. Huang, Z. Chen, et al., Organic Electronics **46**, 22 (2017).
[5] J. Burschka, M. K. Nazeeruddin, M. Gratzel, Nature **499**, 316 (2013).
[6] K. A. Bush, A. F. Palmstrom, M. D. McGehee, et al., Nature Energy **2**, 17009 (2017).
[7] Ch. S. Lai, Y. Jia, L. L. Lai, et al., Renewable and Sustainable Energy Reviews **78**, 439 (2017).
[8] M. Hauck, T. Ligthart, M. Schaap, et al., Renewable Energy **111**, 906 (2017).
[9] M. Xu, J. Feng, Z. J. Fan, et al., Solar Energy Materials and Solar Cells **169**, 8 (2017).
[10] S. Z. Pang, D. Z. Chen, C. F. Zhang, et al., Solar Energy Materials and Solar Cells **170**, 278 (2017).
[11] F. Han, J. S. Luo, H. A. Malik, et al., Journal of Power Sources **359**, 577 (2017).
[12] Michael Gratzel, Nature Materials **13**, 838 (2014).
[13] W. S. Yang, J. H. Noh, S. I. Seok, et al., Science **348**, 1234 (2015).
[14] H. J. Snaith, A. Abate, J. M. Ball, et al., Journal of Physical Chemistry Letters **5**(9), 1511 (2014).
[15] R. Gottes, Am. E. Haltzi, L. Gouda, et al., Journal of Physical Chemistry Letters **5**(15), 2662 (2014).
[16] E. J. Juarez-Perez, R. S. Sanchez, L. Badia, et al., Journal Physical Chemistry Letters **5**(13), 2390 (2014).
[17] G. Murugadoss, R. Thangamuthu, M. R. Kumar, et al., Materials Letters **205**, 130 (2017).
[18] Q. J. Liu, L. S. Fan, Q. E. Zhang, et al., CHEMSUSCHEM **10**(15), 3098 (2017).
[19] M. Wong-Stringer, J. E. Bishop, J. A. Smith, et al., Journal of Materials Chemistry A **5**(30), 15714 (2017).

[20] L. Li, N. Liu, H. P. Zhou, et al., ACS Nano, 2017, DOI :10.1021/acsnano.7b02867.

[21] J. H. Heo, S. H. Im, S. Il. Seok, et al., Nature Photonics **7**(7), 486 (2013).

[22] W. S. Yang, J. H. Noh, S. Il. Seok, et al., Science **348**(6240), 1234 (2015).

[23] P. Gao, M. Gtatzel, M. K. Nazeeruddin, Energy & Environmental Science **7**, 2448 (2014).

[24] Y. G. Tu, J. H. Wu, X. He, et al., Applied Surface Science **403**, 572 (2017).

[25] W. Kong, Z. Ye, H. Wu, et al., Physical Chemistry Chemical Physics **17**, 16405 (2015).

[26] M. Namatame, M. Yabusaki, K. Marumoto, et al., Applied Physics Letters **110**, 123904 (2017).

[27] J. Xiong, Z. He, S. P. Zhan, et al., Physica Status Solidi A-Applications and Materials Science **214**(10), 1700281 (2017).

[28] G. Liu, H. Zhou, Q. Chen, et al., Crystals **8**(5), 185 (2018).

---

*Corresponding author: water198966@hotmail.com